INTERNATIONAL JOURNAL FOR NUMERICAL METHODS IN FLUIDS, VOL. 14, 883–905 (1992)

THE DOUBLE von MISES TRANSFORMATION IN THE STUDY OF TWO-PHASE FLUID FLOW OVER CURVED BOUNDARIES: THEORY AND ANALYSIS

R. M. BARRON

Department of Mathematics and Statistics, and Fluid Dynamics Research Institute, University of Windsor, Windsor, Ontario, Canada N9B 3P4

AND

M. H. HAMDAN*

Department of Mathematics and Computer Science, Mount Allison University, Sackville, New Brunswick, Canada E0A 3C0

SUMMARY

A numerical method to handle the flow of a two-phase fluid over curved boundaries is proposed. The method is based on the double von Mises transformation which is derived in this work and is expected to be applicable to a variety of flow situations while utilizing the finite difference technique. In order to illustrate the numerical implementation of the method, dusty fluid flow through a porous channel possessing curved boundaries and the flow through a semi-infinite porous layer overlying a curved lower boundary are considered. The flow is assumed to be governed by model equations based on Brinkman's equation and reflecting boundary conditions are employed in the study based on a uniform dust particle distribution. Results indicate that an increase in the permeability results in decreasing the tangential velocity component in regions close to the curved boundary, and increasing the dust parameters decreases this component. The effects of the grid size and the extent of the computational domain are discussed. The results also shed some light on the applicability of the dusty fluid flow model and suggest that the model is best employed when the permeability is high, a conclusion that is consistent with the validity of Brinkman's equation.

KEY WORDS Von Mises transformation Curved boundaries Numerical solution Two-phase fluid flow

1. INTRODUCTION

The literature cites numerous numerical procedures and models that are applicable to the study of multiphase fluid flow systems. In particular, Crowe[1] reports some of the numerical models that have been employed in the study of gas–particulate flow. Most of the reported methods rely heavily on the use of the popular finite differences method which, attractive as it may be, is impractical in handling cases where the boundaries are arbitrarily curved.

In order to overcome some of the problems arising due to the presence of curved boundaries and yet employ the finite difference technique, this study offers an alternative approach that is based on the transformation of the governing equations using the von Mises transformation. The

* Present address: Division of MECS, The University of New Brunswick, P.O. Box 5050, Saint John, N.B., Canada E2L 4L5.

0271–2091/92/080883–23$11.50
© 1992 by John Wiley & Sons, Ltd.
Received November 1989
Revised July 1991

numerical solution is obtained in the computational domain through the use of the finite difference technique.

Although this work is concerned primarily with developing the transformation that is applicable to two-phase fluid flow systems, a basic understanding of the von Mises transformation suitable for the study of single-phase fluid flow is essential and is also offered in this work in its more general, time-dependent form. This is followed by derivation of the double von Mises transformation that is proposed in this work to be applicable to the study of two-phase fluid flow over curved boundaries.

The double von Mises extension is not only of great utility in the study of dusty fluid flow through porous media but also represents a major step in the study of general dusty gas flow in free space. One of its main objectives is to facilitate the study of the complicated problem of flow of a dusty fluid through domains with arbitrarily curved boundaries. It can also simplify matters in the study of dusty gas flow in rectangular domains. In this case the dust phase equations are only transformed in terms of the von Mises variables. It should be noted that when the dusty fluid flow is considered in rectangular domains, interchanging the independent variable Y with the streamfunction Ψ in the dust phase equations has been reported by Soo.[2] The current extended von Mises approach represents a more general method, of which the method followed by Soo is a special case.

In order to illustrate the applicability of the extended von Mises approach, we consider the dusty fluid flow through two different porous domains: a semi-infinite porous block bounded below by a fluid of very high viscosity, termed here stationary or static fluid, and a porous channel possessing curved boundaries. This type of (static) boundary is chosen so that the Jacobian of the transformation associated with the fluid phase equations remains finite.

The equations governing the flow in the described domain are based on a model that has been developed by Hamdan and Barron,[3] which describes the flow of a dusty fluid in porous media based on Brinkman's model. One of the main physical applications of this model is that given the macroscopic distribution of the dust particle number density, it is possible to solve the model equations to obtain the conditions under which this distribution is possible. In the current work the model equations are employed to study the effect of introducing a uniform distribution of the dust particles (in the porous medium) on the fluid flow characteristics. Although in a typical gas–particulate flow problem in porous media the dust particles might undergo a variety of conditions leading to various capture, straining and settling mechanisms of the particles on the solid grains of the porous matrix—and hence the assumption of a uniform distribution of dust particles in the domain is indeed restrictive—the current problem nevertheless offers an initial step in the understanding of the more general problem of variable dust particle distribution. However, the proposed method of solution is extensible, as discussed in Section 9, to handle the variable distribution problem.

2. THE von MISES TRANSFORMATION AND SINGLE-PHASE FLUID FLOW

In 1927 von Mises[4] introduced a co-ordinate transformation, now recognized as the von Mises transformation, to transform the two-dimensional boundary layer equations into a form in which the independent variables X and Y are replaced by X and Ψ respectively, where Ψ is the streamfunction.

Although the von Mises transformation has been known for over half a century, it has mainly been of considerable importance in theoretical boundary layer investigations.[5] In a deviation from boundary layer analysis, Benjamin[6] employed the transformation in his study of solitary waves with arbitrary vorticity distribution.

Numerical implementation of the von Mises transformation came about when Barron[7] presented a formulation and computations involving von Mises variables in his study of flow over aerofoils of arbitrary shapes as a substitute for grid generation. His analysis showed that the von Mises transformation can be arrived at through Martin's approach,[8] of which the von Mises transformation is a special case, obtained by a 'judicious choice of the co-ordinate curves'.

The success of the transformation in the numerical study of a particular flow problem relies heavily on the requirement that each of the boundaries of the flow domain remains a streamline or part of a streamline. The streamlines $\Psi = \text{constant}$, which may not be straight lines in the physical plane, are mapped into horizontal straight lines in the transformed plane and Ψ replaces the original independent variable.

The problem of determining Ψ in the physical plane is replaced by the problem of determining Y in the rectangular computational plane. Other flow variables of interest (velocity, pressure and vorticity) become, in the computational plane, functions of X and Ψ. The method of solution for a particular problem is to transform the governing equations into the new co-ordinate system so that the curved boundaries of the physical domains are transformed into straight lines, with the whole of the domain being thus transformed into a rectangular region, designated the computational domain.

Two methods are possible to transform the governing equations into the new co-ordinates. The first relies on the direct transformation of the derivatives and the primitive variables involved by using the transformation operators which are discussed in this section. In this case the pressure terms are treated through the introduction of an energy function and the resulting equations are cast in vorticity–Y form. Details of this method are explained in the work of Barron.[7] The second approach is to cast the governing equations in vorticity–streamfunction form and then to transform these equations in terms of the new co-ordinate transformation. This second approach is implemented here.

Let Ψ represent the streamfunction of a two-dimensional flow and U and V represent the horizontal and vertical velocity components, given in terms of Ψ by

$$U = \Psi_Y, \qquad V = -\Psi_X, \tag{1}$$

and let Ω represent the vorticity, given in terms of the velocity components by

$$\Omega = V_X - U_Y, \tag{2}$$

where, throughout this work, subscript notation denotes partial differentiation.

We now consider the two-dimensional transformation of co-ordinates between the Cartesian co-ordinates (X, Y) and time T and the curvilinear co-ordinates (Φ, Ψ) and time τ, defined by

$$\Phi = \Phi(X), \tag{3}$$

$$\Psi = \Psi(X, Y, T), \tag{4}$$

$$\tau = \tau(T). \tag{5}$$

Expanding (3)–(5) by the chain rule, the following expressions are obtained:

$$\partial_X = \Phi_X \partial_\Phi + \Psi_X \partial_\Psi + \tau_X \partial_\tau, \tag{6}$$

$$\partial_Y = \Phi_Y \partial_\Phi + \Psi_Y \partial_\Psi + \tau_Y \partial_\tau, \tag{7}$$

$$\partial_T = \Phi_T \partial_\Phi + \Psi_T \partial_\Psi + \tau_T \partial_\tau. \tag{8}$$

Taking $X=\Phi$ and $T=\tau$, equations (6)–(8) take the form

$$\partial_X=\partial_\Phi+\Psi_X\partial_\Psi, \tag{9}$$

$$\partial_Y=\Psi_Y\partial_\Psi, \tag{10}$$

$$\partial_T=\partial_\tau+\Psi_T\partial_\Psi. \tag{11}$$

The spatial Jacobian of the above transformation is given by

$$J_1=\frac{\partial(X, Y)}{\partial(\Phi, \Psi)}=Y_\Psi, \tag{12}$$

while the temporal Jacobian of the transformation is given by

$$J_2=\frac{\partial(X, Y)}{\partial(\Phi, \tau)}=Y_\tau. \tag{13}$$

It should be noted at this point that if $J_1=0$ or is infinite, or equivalently $Y_\Psi=0$ or is infinite, then the transformation is singular. If $J_2\equiv 0$, or equivalently $Y_\tau\equiv 0$, then the transformation reduces to the steady transformation, i.e. the usual von Mises transformation. If, however, $0<|J_1|<\infty$ and $0<|J_2|<\infty$, then equations (3)–(5) with $X=\Phi$ and $T=\tau$ can be solved for Ψ_X, Ψ_Y and Ψ_T in terms of the first derivatives of Y to give the expressions

$$\Psi_T=-Y_\tau/Y_\Psi=-J_2/J_1, \tag{14}$$

$$\Psi_X=-Y_\Phi/Y_\Psi=-Y_\Phi/J_1, \tag{15}$$

$$\Psi_Y=1/Y_\Psi=1/J_1. \tag{16}$$

Substituting (14)–(16) into (9)–(11), the following first-derivative expressions in the new co-ordinate system are obtained, where the independent variable Φ is replaced by its equivalent X and τ is replaced by T:

$$\partial_X=\partial_X-(Y_X/Y_\Psi)\partial_\Psi, \tag{17}$$

$$\partial_Y=(1/Y_\Psi)\partial_\Psi, \tag{18}$$

$$\partial_T=\partial_T-(Y_T/Y_\Psi)\partial_\Psi. \tag{19}$$

The following expressions for the second-order spatial derivatives can also be obtained in the new co-ordinate system by applying the above operators on themselves:

$$\partial_{XX}=\partial_{XX}-2(Y_X/Y_\Psi)\partial_{X\Psi}+(Y_X/Y_\Psi)^2\partial_{\Psi\Psi}+(2Y_X Y_{X\Psi}/Y_\Psi^2-Y_{XX}/Y_\Psi-Y_X^2 Y_{\Psi\Psi}/Y_\Psi^3)\partial_\Psi, \tag{20}$$

$$\partial_{YY}=(1/Y_\Psi^2)\partial_{\Psi\Psi}-(Y_{\Psi\Psi}/Y_\Psi^3)\partial_\Psi \tag{21}$$

The cross-derivative takes the form

$$\partial_{XY}=(Y_X/Y_\Psi^3)\partial_{\Psi\Psi}+[(Y_X Y_{\Psi\Psi}-Y_\Psi Y_{X\Psi})/Y_\Psi^3]\partial_\Psi. \tag{22}$$

Once the equations governing single-phase fluid flow are expressed in terms of the two-dimensional streamfunction and vorticity and the above differential operators are applied, then the roles of the dimensionless streamfunction and the independent variable Y have been interchanged to yield new independent variables X, Ψ and T in terms of which the flow variables are to be expressed. The governing equation that the streamfunction Ψ satisfies will be transformed into an equation that the new dependent variable Y satisfies, where $Y=Y(X, \Psi, T)$. Furthermore, other flow variables that are originally functions of X, Y and T and satisfy the governing

equations in Ω–Ψ form become functions of the new independent variables X, Ψ and T and thus satisfy the governing equations in the transformed Ω–Y form.

To this end the two-dimensional velocity components U and V defined by equations (1) are transformed using equations (9) and (10) to yield

$$U = 1/Y_\Psi, \tag{23}$$

$$V = Y_X/Y_\Psi = U Y_X. \tag{24}$$

3. APPLICATION OF TRANSFORMATION EQUATIONS TO NAVIER–STOKES EQUATIONS

In order to illustrate the structure of the transformed equations, we apply the above-derived single-co-ordinate transformation to the Navier–Stokes equations. These equations are considered here for the unsteady flow of an incompressible, viscous fluid in the following dimensionless vorticity–streamfunction form:

streamfunction equation,

$$\Omega = -\Psi_{XX} - \Psi_{YY}; \tag{25}$$

vorticity equation,

$$\Omega_T + \Psi_Y \Omega_X - \Psi_X \Omega_Y = (\Omega_{XX} + \Omega_{YY})/Re. \tag{26}$$

Applying the operators (17)–(21) to equations (25) and (26), we get

$$Y_\Psi^2 Y_{XX} - 2Y_X Y_\Psi Y_{X\Psi} + (1 + Y_X^2) Y_{\Psi\Psi} = Y_\Psi^3 \Omega, \tag{27}$$

$$\Omega_T = [Y_\Psi^2 \Omega_{XX} - 2Y_X Y_\Psi \Omega_{X\Psi} + (1 + Y_X^2)\Omega_{\Psi\Psi}]/Re\, Y_\Psi^2 - \Omega\Omega_\Psi/Re + (Y_T \Omega_\Psi - \Omega_X)/Y_\Psi. \tag{28}$$

4. THE EXTENDED von MISES TRANSFORMATION AND DUSTY GAS FLOW

In Section 2 the von Mises transformation was extended to include the time derivative so as to facilitate studies of unsteady flow problems over curved boundaries. Successful application of the steady von Mises transformation to single-phase fluid flow problems over curved boundaries[7,9] gives rise to the idea of extending the von Mises transformation even further in an attempt to offer a method that is capable of treating the general two-phase fluid flow over curved boundaries.

Consider the two sets of transformations between the Cartesian co-ordinates (X_1, Y_1) and time T_1 and the curvilinear co-ordinates (Φ_1, Ψ_1) and time τ_1, and between the Cartesian co-ordinates (X_2, Y_2) and time T_2 and the curvilinear co-ordinates (Φ_2, Ψ_2) and time τ_2, defined by

$$X_1 = \Phi_1, \tag{29}$$

$$Y_1 = Y_1(\Phi_1, \Psi_1, \tau_1), \tag{30}$$

$$T_1 = \tau_1 \tag{31}$$

and

$$X_2 = \Phi_2, \tag{32}$$

$$Y_2 = Y_2(\Phi_2, \Psi_2, \tau_2), \tag{33}$$

$$T_2 = \tau_2, \tag{34}$$

with $X_1 = X_2$, $T_1 = T_2$ and $Y_1 = Y_2$ in the physical plane.

The Jacobians of the transformations are given by

$$J_{1S}=\frac{\partial(X_1, Y_1)}{\partial(\Phi_1, \Psi_1)}=(Y_1)_{\Psi_1}, \tag{35}$$

$$J_{2S}=\frac{\partial(X_2, Y_2)}{\partial(\Phi_2, \Psi_2)}=(Y_2)_{\Psi_2}, \tag{36}$$

$$J_{1T}=\frac{\partial(X_1, Y_1)}{\partial(\Phi_1, \tau_1)}=(Y_1)_{\tau_1}, \tag{37}$$

$$J_{2T}=\frac{\partial(X_2, Y_2)}{\partial(\Phi_2, \tau_2)}=(Y_2)_{\tau_2}, \tag{38}$$

where the subscripts S and T indicate spatial and temporal respectively.

It is clear that if $J_{1S}=0$ or is infinite, then the first transformation is singular, while if $J_{1T}\equiv 0$, then the first transformation reduces to the steady von Mises transformation. Similar conclusions can be drawn about the second transformation. If, however, $0<|J_{1S}|<\infty$ and $0<|J_{1T}|<\infty$, then (29)–(31) define a one-to-one transformation. Similarly, if $0<|J_{2S}|<\infty$ and $0<|J_{2T}|<\infty$, then (32)–(34) define a one-to-one transformation.

Using a similar analysis to that used in obtaining equations (17)–(19) reveals that partial derivatives in the two co-ordinate systems in the first transformation are related by

$$\partial_{T_1}=\partial_{\tau_1}-[(Y_1)_{\tau_1}/(Y_1)_{\Psi_1}]\partial_{\Psi_1}, \tag{39}$$

$$\partial_{X_1}=\partial_{\Phi_1}-[(Y_1)_{\Phi_1}/(Y_1)_{\Psi_1}]\partial_{\Psi_1}, \tag{40}$$

$$\partial_{Y_1}=[1/(Y_1)_{\Psi_1}]\partial_{\Psi_1}, \tag{41}$$

while partial derivatives of the two co-ordinate systems in the second transformation are related by

$$\partial_{T_2}=\partial_{\tau_2}-[(Y_2)_{\tau_2}/(Y_2)_{\Psi_2}]\partial_{\Psi_2}, \tag{42}$$

$$\partial_{X_2}=\partial_{\Phi_2}-[(Y_2)_{\Phi_2}/(Y_2)_{\Psi_2}]\partial_{\Psi_2}, \tag{43}$$

$$\partial_{Y_2}=[1/(Y_2)_{\Psi_2}]\partial_{\Psi_2}. \tag{44}$$

According to (29) and (32), we consider $X_1=\Phi_1$ and $X_2=\Phi_2$. Together with the fact that $X_1=X_2$ in the physical plane, we conclude that $\Phi_1=\Phi_2$ in the computational plane. Likewise, according to (31) and (34), we take $T_1=\tau_1$ and $T_2=\tau_2$. Since $T_1=T_2$, we must have $\tau_1=\tau_2$.

In the case of Y_1 and Y_2 the situation is different. From (30) and (33), $Y_1=Y_1(X, \Psi_1, T)$ and $Y_2=Y_2(X, \Psi_2, T)$ in the computational plane. The fact that $Y_1=Y_2$ in the physical plane does not necessarily imply that $Y_1=Y_2$ in the computational plane. This is due to the fact that the equations governing Y_1 and Y_2 in the computational plane are different. This is clarified further in the following discussion.

The differential operators given by (39)–(41) will thus transform a given differential equation from the physical (X_1, Y_1) plane to the computational (Φ_1, Ψ_1) plane. The differential operators given by (42)–(44) will transform a given differential equation from the physical (X_2, Y_2) plane to the computational (Φ_2, Ψ_2) plane.

So far no connection has been assumed between the governing equations in the physical plane or between the first and second transformations derived above. In order to make this connection,

we assume that we are given, in the physical plane, coupled partial differential equations governing two-phase fluid flow. For the first phase we have a streamfunction equation given in terms of Ψ_1 as a function of the two-dimensional co-ordinates X and $Y (= Y_1)$ and time T. This streamfunction equation is coupled with the first-phase vorticity equation which is given in terms of Ω_1 as a function of X and Y and time T. Similarly, for the second phase we assume that we have a streamfunction equation in terms of Ψ_2 which is a function of X and $Y (= Y_2 = Y_1)$ and time T. The streamfunction equation is coupled with the second-phase vorticity equation in terms of Ω_2 as a function of X, Y and T. The two phases are coupled together through the vorticity of each of the phases.

In the physical plane it is required to solve the coupled equations simultaneously to determine the flow variables $\Psi_1(X, Y, T)$, $\Psi_2(X, Y, T)$, $\Omega_1(X, Y, T)$ and $\Omega_2(X, Y, T)$. By using the double transformation derived above, the flow equations are transformed from the physical plane into a computational plane where Ψ_1 becomes an independent variable when the first-phase equations are transformed and Ψ_2 becomes an independent variable when the second-phase equations are transformed. Since in the physical plane the two phases coexist—in other words we only have one physical plane—the one-to-one mapping from/to the physical plane to/from the computational plane necessitates the existence of a single computational domain. Therefore, if the transformation of the governing equations is at all possible, then interchanging Ψ_1 and Y, and Ψ_2 and Y must be such that the grid lines $\Psi_1 = \text{constant}$ and $\Psi_2 = \text{constant}$ coincide in the computational plane. In this case it is possible to generate a one-to-one mapping from the physical plane to the computational plane.

However, it is important to note that images of $\Psi_1 = \text{constant}$ and $\Psi_2 = \text{constant}$ do not necessarily coincide in the physical domain. These image lines represent the first-phase and second-phase streamlines respectively. Once the roles of the dependent variable Ψ_1 and the independent variable Y are interchanged, the first-phase governing equations are given in terms of Ω_1 and Y, where $Y = Y(X, \Psi_1)$ and $\Omega_1 = \Omega_1(X, \Psi_1)$. Similarly, for the second phase the equations are given in terms of Ω_2 and Y, where $Y = Y(X, \Psi_2)$ and $\Omega_2 = \Omega_2(X, \Psi_2)$. Thus we have $Y = Y(X, \Psi_1)$, where Y is governed by the Y-equation due to the first phase. Similarly, $Y = Y(X, \Psi_2)$, where Y is governed by the Y-equation due to the second phase. We also know that the lines $\Psi_1 = \text{constant}$ and $\Psi_2 = \text{constant}$ coincide in the computational plane. This might lead to the apparent conclusion that the computed Y is the same. This, of course, is untrue, since Y is governed by two different partial differential equations and therefore the solution to each of the equations renders a value for Y that is different from the other. This can be compared to obtaining a coupled solution to two different flow variables that are functions of the same independent variables. If the partial differential equations are different, then the solution for each of the two flow variables is different.

In terms of the physical plane terminology we can say that: in a given flow problem of a two-phase fluid the first-phase streamlines are different from the second-phase streamlines. The governing partial differential equations are to be solved to determine, say, the shape of the streamlines. In terms of the computational domain we have the following analogy. Given $\Psi_1 = \Psi_2 = \text{constant} = \sigma$, determine the second-phase value of Y on a given grid line and call the solution Y_2. Then determine the first-phase value of Y on the same grid line and call it Y_1. Plotting these two different values of Y gives the shape of the first-phase streamline $\Psi_1 = \sigma$ and the shape of the second-phase streamline $\Psi_2 = \sigma$.

At this point, in order to implement the transformation equations given by (39)–(44) and for convenience of notation, Φ_1 and Φ_2 are replaced by X, τ_1 and τ_2 are replaced by T and Ψ_1 and Ψ_2 are replaced by Ψ. Equations (39)–(44) will thus take the following equivalent form:

for the first transformation,

$$\partial_T = \partial_T - [(Y_1)_T/(Y_1)_\Psi]\partial_\Psi, \tag{45}$$

$$\partial_X = \partial_X - [(Y_1)_X/(Y_1)_\Psi]\partial_\Psi, \tag{46}$$

$$\partial_Y = [1/(Y_1)_\Psi]\partial_\Psi; \tag{47}$$

for the second transformation,

$$\partial_T = \partial_T - [(Y_2)_T/(Y_2)_\Psi]\partial_\Psi, \tag{48}$$

$$\partial_X = \partial_X - [(Y_2)_X/(Y_2)_\Psi]\partial_\Psi, \tag{49}$$

$$\partial_Y = [1/(Y_2)_\Psi]\partial_\Psi. \tag{50}$$

5. APPLICATION OF THE DOUBLE TRANSFORMATION TO SAFFMAN'S DUSTY GAS FLOW EQUATIONS

In order to illustrate the structure of the transformed equations, the above double transformation is applied to the equations governing the flow of a dusty fluid as given by Saffman.[10] Saffman's equations which, when the fluid phase is incompressible and the number density of the dust is constant, take the following dimensionless vorticity–streamfunction form:

for the fluid phase,

$$\Omega_1 = -(\Psi_1)_{XX} - (\Psi_1)_{YY}, \tag{51}$$

$$Re[(\Psi_1)_Y(\Omega_1)_X - (\Psi_1)_X(\Omega_1)_Y] = (\Omega_1)_{XX} + (\Omega_1)_{YY} + Re\,Sn(\Omega_2 - \Omega_1); \tag{52}$$

for the dust phase,

$$\Omega_2 = -(\Psi_2)_{XX} - (\Psi_2)_{YY}, \tag{53}$$

$$(\Psi_2)_Y(\Omega_2)_X - (\Psi_2)_X(\Omega_2)_Y = (\Omega_1 - \Omega_2)S/M. \tag{54}$$

Here the dimensionless quantities Ψ_1 and Ψ_2 are the fluid phase and dust phase streamfunctions respectively, Ω_1 and Ω_2 are the respective vorticities, n is the particle number density, S/M is the relaxation time, S is the Stokes coefficient of resistance, M is the mass of each dust particle and Re is the Reynolds number.

Upon applying the first-transformation operators (46) and (47) to the fluid phase equations (51) and (52) while applying the second-transformation operators (49) and (50) to the dust phase equations (53) and (54), the following transformed equations are obtained:

for the fluid phase,

$$(Y_1)_\Psi^2(Y_1)_{XX} - 2(Y_1)_X(Y_1)_\Psi(Y_1)_{X\Psi} + [1 + (Y_1)_X^2](Y_1)_{\Psi\Psi} = (Y_1)_\Psi^3\Omega_1, \tag{55}$$

$$(Y_1)_\Psi^2(\Omega_1)_{XX} - 2(Y_1)_X(Y_1)_\Psi(\Omega_1)_{X\Psi} + [1 + (Y_1)_X^2](\Omega_1)_{\Psi\Psi} = \Omega_1(Y_1)_\Psi^2(\Omega_1)_\Psi + Re\,Sn(Y_1)_\Psi^2(\Omega_1 - \Omega_2) + Re(Y_1)_\Psi(\Omega_1)_X; \tag{56}$$

for the dust phase,

$$(Y_2)_\Psi^2(Y_2)_{XX} - 2(Y_2)_X(Y_2)_\Psi(Y_2)_{X\Psi} + [1 + (Y_2)_X^2](Y_2)_{\Psi\Psi} = (Y_2)_\Psi^3\Omega_2, \tag{57}$$

$$(\Omega_2)_X = (Y_2)_\Psi(\Omega_1 - \Omega_2)S/M. \tag{58}$$

6. APPLICATION TO DUSTY FLUID FLOW THROUGH POROUS MEDIA

6.1. Problem formulation

We consider the dusty fluid flow through a semi-infinite porous medium that is bounded below by a stationary (static) fluid as shown in Figure 1. The interface between the static fluid and the porous medium is assumed to be known, for the sake of simplicity, and takes the form $Y=f(X)$ in the Cartesian plane, where $f(X)$ is the smooth function given by

$$f(X)=\begin{cases}0{\cdot}2(0{\cdot}25-X^2)^{1/2}, & -0{\cdot}5\leqslant X\leqslant 0{\cdot}5,\\ 0, & X<-0{\cdot}5 \text{ or } X>0{\cdot}5.\end{cases} \tag{59}$$

It is further assumed that there is no momentum or mass transfer between the dusty fluid in the porous medium and the static fluid; thus the interface may be considered a streamline of the flow as discussed below. This physical situation of a porous medium overlying a stationary fluid can be realized if one considers a stationary fluid of a much higher viscosity than that of the fluid phase in the porous medium. The choice here is made so that the spatial Jacobian of the transformation, as applied to the fluid phase, does not become infinite. This situation is ascertained by the tangency condition that is used in conjunction with the chosen lower boundary. It should be noted that if the lower bounding fluid is not of high viscosity, then momentum and mass transfer between the dusty fluid in the porous medium and the bounding fluid has to be taken into

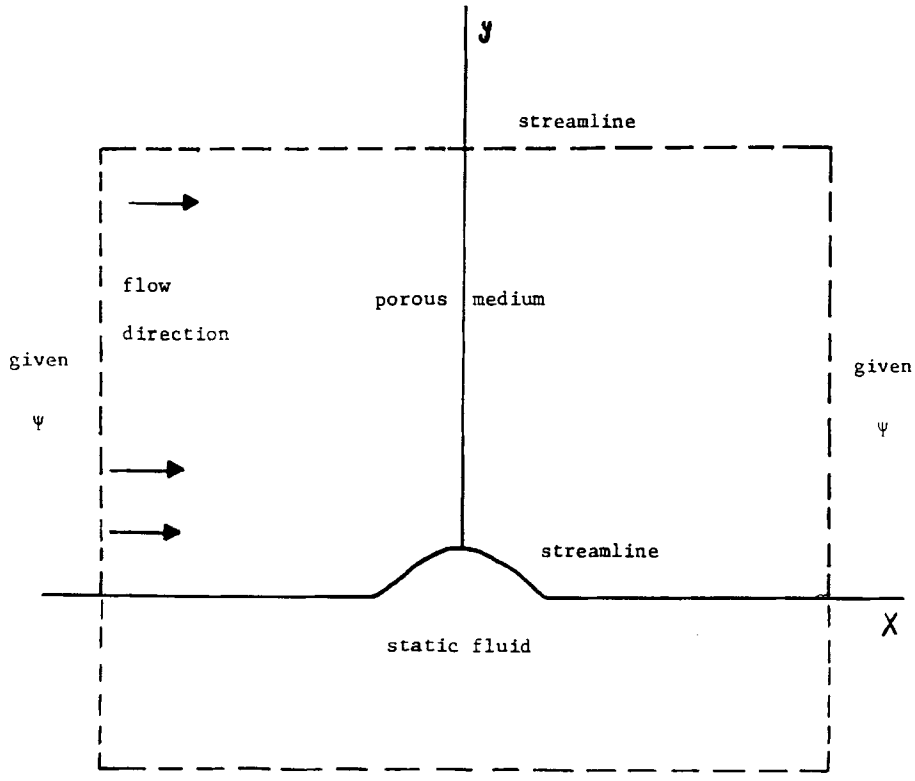

Figure 1. Representative sketch: physical domain

consideration. In this case the interface between the two domains does not necessarily represent a streamline of the flow. Although it can be argued that the method of double von Mises transformation is still applicable in this case, the situation necessitates a knowledge of the boundary conditions along the interface.

6.2. *Governing equations*

The steady, rotational, laminar plane flow of an incompressible, viscous dusty fluid through porous media is governed by the following macroscopic differential equations:

for the fluid phase,

$$\nabla \cdot \mathbf{u} = 0 \quad \text{(conservation of mass)}, \tag{60}$$

$$-\nabla p + \mu \nabla^2 \mathbf{u} + (\mathbf{v} - \mathbf{u})(KN + \mu/\eta^*) = \mathbf{0} \quad \text{(conservation of linear momentum)}; \tag{61}$$

for the dust phase,

$$\nabla \cdot \mathbf{v} = 0 \quad \text{(conservation of mass)}, \tag{62}$$

$$mN(\mathbf{v} \cdot \nabla)\mathbf{v} = -\nabla p^* + KN(\mathbf{u} - \mathbf{v}) \quad \text{(conservation of linear momentum)}. \tag{63}$$

Here $\mathbf{u}$ is the fluid phase macroscopic velocity vector, $\mathbf{v}$ is the dust phase macroscopic velocity vector, p is the fluid pressure, p^* is the dust phase partial pressure, μ is the viscosity, η^* is the permeability, m is the mass of each dust particle, K is the drag coefficient of resistance and N is the dust particle number density.

For the two-dimensional flow under consideration, equations (60)–(63) represent a system of six equations in the seven unknowns u, $\mathbf{v}$, N, p and p^*. Assuming a uniform distribution of dust particles throughout the flow field, the number density N can be taken as constant, reducing the number of unknowns to six. The dust phase partial pressure p^* is the pressure necessary for the computed dust phase velocity components to satisfy equation (63) with N taken as constant.[11]

Eliminating the pressure terms, equations (60)–(63) can be expressed in the following (non-dimensional) vorticity–streamfunction form:

for the fluid phase,

$$\Omega_1 = -(\Psi_1)_{XX} - (\Psi_1)_{YY}, \tag{64}$$

$$(\Omega_1)_{XX} + (\Omega_2)_{YY} + [(KN)^* Re + 1/\eta](\Omega_2 - \Omega_1) = 0; \tag{65}$$

for the dust phase,

$$\Omega_2 = -(\Psi_2)_{XX} - (\Psi_2)_{YY}, \tag{66}$$

$$(\Psi_2)_Y(\Omega_2)_X - (\Psi_2)_X(\Omega_2)_Y = K_1(\Omega_1 - \Omega_2). \tag{67}$$

Here Ψ_1 is the fluid phase streamfunction, Ψ_2 is the dust phase streamfunction, Ω_1 is the fluid phase vorticity and Ω_2 is the dust phase vorticity.

The non-dimensional quantities in equations (64)–(67) are related to the original dimensional quantities by the following relations: $\mathbf{U} = \mathbf{u}/U_0$, $\mathbf{V} = \mathbf{v}/U_0$, $X = x/L$, $Y = y/L$, $\eta = \eta^*/L^2$, $(KN)^* = KN/(\rho U_0/L)$, $K_1 = K/(mL/U_0)$, $Re = LU_0\rho/\mu$ is the Reynolds number, where U_0 and L are characteristic velocity and length respectively.

In terms of the streamfunctions the dimensionless velocity components are defined by

$$U_1=(\Psi_1)_Y, \qquad U_2=(\Psi_2)_Y, \tag{68}$$

$$V_1=-(\Psi_1)_X, \qquad V_2=-(\Psi_2)_X \tag{69}$$

and the dimensionless vorticities are defined by

$$\Omega_1=(V_1)_X-(U_1)_Y, \tag{70}$$

$$\Omega_2=(V_2)_X-(U_2)_Y. \tag{71}$$

In the type of flow and porous medium under consideration the effects of Re are negligible and thus (65) takes the form

$$(\Omega_1)_{XX}+(\Omega_2)_{YY}+(1/\eta)(\Omega_2-\Omega_1)=0. \tag{72}$$

The dusty fluid flow equations (64), (66), (67) and (72) are then transformed into the new co-ordinate system by applying the transformation equations (46) and (47) to the fluid phase equations and the transformation equations (49) and (50) to the dust phase equations.

The fluid phase streamfunction equation (64) is thus transformed to the form

$$(Y_1)_\Psi^2(Y_1)_{XX}-2(Y_1)_X(Y_1)_\Psi(Y_1)_{X\Psi}+[1+(Y_1)_X^2](Y_1)_{\Psi\Psi}=(Y_1)_\Psi^3\Omega_1. \tag{73}$$

The dust phase streamfunction equation (66) is also transformed to a form similar to (73).

The dust phase vorticity equation (67) is transformed into

$$(\Omega_2)_X=K_1(Y_2)_\Psi(\Omega_1-\Omega_2), \tag{74}$$

while the fluid phase vorticity equation (72) is transformed to

$$(Y_1)_\Psi^2(\Omega_1)_{XX}-2(Y_1)_X(Y_1)_\Psi(\Omega_1)_{X\Psi}+[1+(Y_1)_X^2](\Omega_1)_{\Psi\Psi}-\Omega_1(Y_1)_\Psi^2(\Omega_1)_\Psi-(Y_1)_\Psi^2(\Omega_2-\Omega_1)/\eta=0. \tag{75}$$

The problem has thus been transformed from that of determining Ψ_1, Ψ_2, Ω_1 and Ω_2 in the physical plane to that of finding Y_1, Y_2, Ω_1 and Ω_2 in the computational plane. Once Y_1 and Y_2 are obtained, then the fluid phase and dust phase streamlines may be simply obtained by plotting the values of Y_1 and Y_2 in the physical (X, Y) plane.

6.3. Boundary conditions

In this work the simple case of uniform flow at infinity for both the dust phase and the fluid phase is employed. Although the uniform flow at $X=-\infty$ is plausible, the uniform flow assumption at $X=\infty$ seems to be improbable in the light of the fact that in the presence of a boundary the dust particles may bombard this boundary, deposit and accumulate on this boundary, initiate the motion of other particles already settled on the boundary or bounce off the boundary and reflect back into the flow field.[11]

Although the above is perfectly acceptable in the case of a solid boundary, the current problem avoids this situation by taking the lower boundary of the porous medium to be a static fluid, along which the usual flow tangency condition can also be interpreted as a no-penetration condition for the dust particles. This implies that the effect of this boundary on the dust particles is to perfectly reflect the dust particles back into the flow field. This of course is facilitated by the assumption that the dust particle number density is constant throughout the flow field, which implies that the static interface may be taken as a dust phase streamline, considered here as the zero streamline for both the fluid and the dust. In the light of this discussion and assuming that

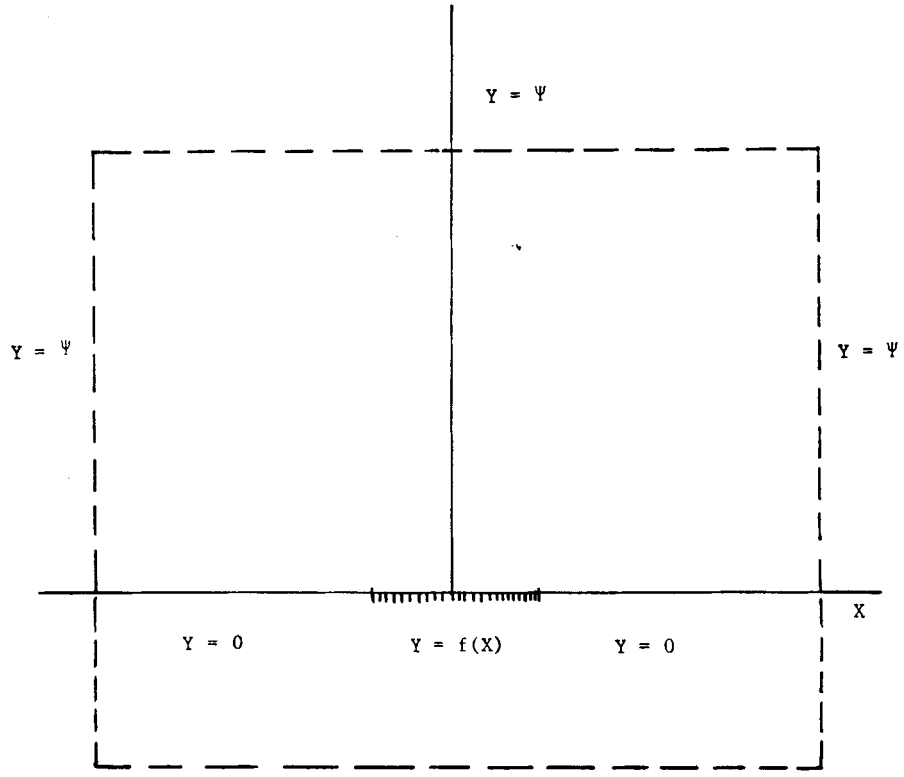

Figure 2. Representative sketch: computational domain

the flow domain is large enough that the effect of the hump $f(X)$ on the flow field dies out far downstream, it is possible to impose a uniform flow condition at $X=\infty$. Although this type of boundary condition is the only one treated in the current analysis, other types of boundary conditions compatible with the dusty fluid flow model at hand are also possible.

To summarize, the boundary conditions in the computational domain (Figure 2) take the following form.

1. Uniform flow at infinity:

$$Y_1=\Psi_1 \quad \text{at } X=\pm\infty \text{ and } \Psi_1=\infty, \tag{76}$$

$$Y_2=\Psi_2 \quad \text{at } X=\pm\infty \text{ and } \Psi_2=\infty, \tag{77}$$

$$\Omega_1=0 \quad \text{at } X=\pm\infty \text{ and } \Psi_1=\infty, \tag{78}$$

$$\Omega_2=0 \quad \text{at } X=\pm\infty \text{ and } \Psi_2=\infty. \tag{79}$$

2. Flow tangency (along the interface):

$$Y_1(X,0)=f(X), \quad -\infty<X<\infty, \tag{80}$$

$$Y_2(X,0)=f(X), \quad -\infty<X<\infty. \tag{81}$$

The vorticity along the interface for each of the phases present remains a quantity to be determined.

7. SOLUTION PROCEDURE

The governing system of equations in the new co-ordinate system is solved iteratively and consecutively by locally freezing the coefficients[7] and central differencing the derivatives involved. The iterative solutions to the resulting matrix equations are obtained via successive line over-relaxation subject to the following convergence criterion: $|F_{i,j}^{n+1} - F_{i,j}^{n}| < 5 \times 10^{-5}$ for all internal grid points (i, j), where n is the iteration level and $F_{i,j}$ stands for any of Ψ_1, Ψ_2, Ω_1 or Ω_2. The velocity components and vorticity of each of the phases involved are updated at the boundary using first-order-accurate single-sided schemes in terms of the most up-to-date values of Y_1 and Y_2.

8. RESULTS AND DISCUSSION

Solutions have been obtained for dust parameter $K_1 = 20$ and 50 and dimensionless permeability $\eta = 0{\cdot}1$, $0{\cdot}01$ and $0{\cdot}001$. It should be noted that all the results in this section are based on a 32×32 grid. The extent of the computational domain is chosen for the current analysis to be $-2 \leqslant X \leqslant 2$ and $0 \leqslant \Psi \leqslant 2$.

Although it might be argued that this grid is too coarse and the extent of the domain is not large enough, they have proven to be fine enough to illustrate the applicability of the method. The effects of the domain extent and grid refinement are discussed in Section 8.4. As a cross-check of the validity and accuracy of the obtained solution, the convergent numerical values were substituted into the continuity equation of each of the phases to ensure that they are satisfied. Continuity equations were satisfied to within an error that is no greater than 5×10^{-5} for all points in the flow field. This of course does not preclude the possibility of some inaccuracies that may arise near the leading and trailing edges of the hump, as is witnessed by the less accurate vorticity results as discussed in Section 8.3. These inaccuracies may be better handled by grid-clustering techniques near these edges as discussed by Barron.[7]

8.1. Flow development

In order to illustrate the differences in the streamline patterns for the fluid phase and the dust phase, the requirement of fine plotting scales becomes essential. For this reason the values of Y_1 and Y_2 are tabulated for different streamlines and different flow regimes. These are given in Tables I and II to illustrate that the extended von Mises method renders the streamlines of the two phases. The values of Y_1 and Y_2 are tabulated for the streamlines $\Psi_1 = \Psi_2 = 0{\cdot}09524$, $0{\cdot}38095$ and $1{\cdot}3333$ for different K_1. Once the data in these tables are plotted, the indicated streamlines for the respective phases result.

8.2. Velocity profiles

Figures 3 and 4 illustrate the fluid phase X-component of velocity along the interface for different permeability and different K_1. In Figure 3 this velocity component is illustrated for $K_1 = 20$ and different η. It is seen that an increase in permeability results in a decrease in this velocity component over $f(X)$.

As is well known, an increase in permeability results in a corresponding increase in the velocity of the fluid in the porous medium. Although this is true for most of the porous medium, the decrease in velocity with increasing permeability in regions close to the lower boundary is attributed to the development of a boundary layer. The thickness of the boundary layer is dependent on the permeability and has been predicted to be of the order of $\sqrt{\eta}$.[12]

Table I. Y_1 and Y_2 on different streamlines ($K_1 = 50$, $\eta = 0{\cdot}01$)

	$\Psi = 0{\cdot}09524$		$\Psi = 0{\cdot}38095$		$\Psi = 1{\cdot}3333$	
X	Y_1	Y_2	Y_1	Y_2	Y_1	Y_2
−2	0·09524	0·09524	0·38095	0·38095	1·3333	1·3333
−1·742	0·09534	0·09532	0·38109	0·38101	1·3306	1·3304
−1·484	0·09578	0·09576	0·38244	0·38237	1·3310	1·3309
−1·226	0·09650	0·09649	0·38470	0·38465	1·3320	1·3319
−0·968	0·09789	0·09792	0·38901	0·38898	1·3335	1·3335
−0·709	0·10135	0·10162	0·39788	0·39785	1·3353	1·3353
−0·452	0·13749	0·13711	0·41381	0·41379	1·3371	1·3371
−0·194	0·17387	0·17385	0·42819	0·42819	1·3383	1·3383
0·065	0·18015	0·18013	0·43131	0·43132	1·3385	1·3385
0·323	0·16028	0·16084	0·42187	0·42188	1·3376	1·3376
0·581	0·10749	0·10707	0·40496	0·40497	1·3358	1·3359
0·839	0·09891	0·09877	0·39256	0·39259	1·3337	1·3338
1·097	0·09693	0·09691	0·38630	0·38634	1·3319	1·3319
1·355	0·09607	0·09607	0·38315	0·38321	1·3305	1·3306
1·613	0·09557	0·09559	0·38147	0·38154	1·3298	1·3300
2	0·09524	0·09524	0·38095	0·38095	1·3333	1·3333

Table II. Y_1 and Y_2 on different streamlines ($K_1 = 20$, $\eta = 0{\cdot}01$)

	$\Psi = 0{\cdot}09524$		$\Psi = 0{\cdot}38095$		$\Psi = 1{\cdot}3333$	
X	Y_1	Y_2	Y_1	Y_2	Y_1	Y_2
−2	0·09524	0·09524	0·38095	0·38095	1·3333	1·3333
−1·742	0·09532	0·09523	0·38114	0·38077	1·3310	1·3300
−1·484	0·09575	0·09564	0·38259	0·38216	1·3320	1·3309
−1·226	0·09649	0·09642	0·38497	0·38464	1·3333	1·3326
−0·968	0·09800	0·09808	0·38937	0·38915	1·3350	1·3346
−0·709	0·10187	0·10304	0·39825	0·39807	1·3369	1·3367
−0·452	0·13702	0·13585	0·41434	0·41412	1·3387	1·3386
−0·194	0·17354	0·17325	0·42889	0·42880	1·3398	1·3398
0·065	0·17988	0·17998	0·43200	0·43202	1·3399	1·3400
0·323	0·16069	0·16192	0·42229	0·42241	1·3389	1·3390
0·581	0·10855	0·10825	0·40517	0·40521	1·3370	1·3372
0·839	0·09873	0·09815	0·39295	0·39297	1·3348	1·3350
1·097	0·09663	0·09644	0·38679	0·38688	1·3327	1·3330
1·355	0·09581	0·09577	0·38361	0·38379	1·3311	1·3315
1·613	0·09539	0·09541	0·38182	0·38206	1·3300	1·3305
2	0·09524	0·09524	0·38095	0·38095	1·3333	1·3333

In the current analysis, although a model based on boundary layer analysis has not been employed, the viscous and boundary effects are nevertheless present and are dependent on the permeability. In the light of this, a reduction in the above-discussed velocity component along the lower boundary with increasing permeability is expected as given in Figure 3.

In Figure 4 this component of velocity is illustrated for $\eta = 0{\cdot}1$ and different K_1. It is seen that increasing K_1 results in decreasing this velocity component over the major part of $f(X)$. This

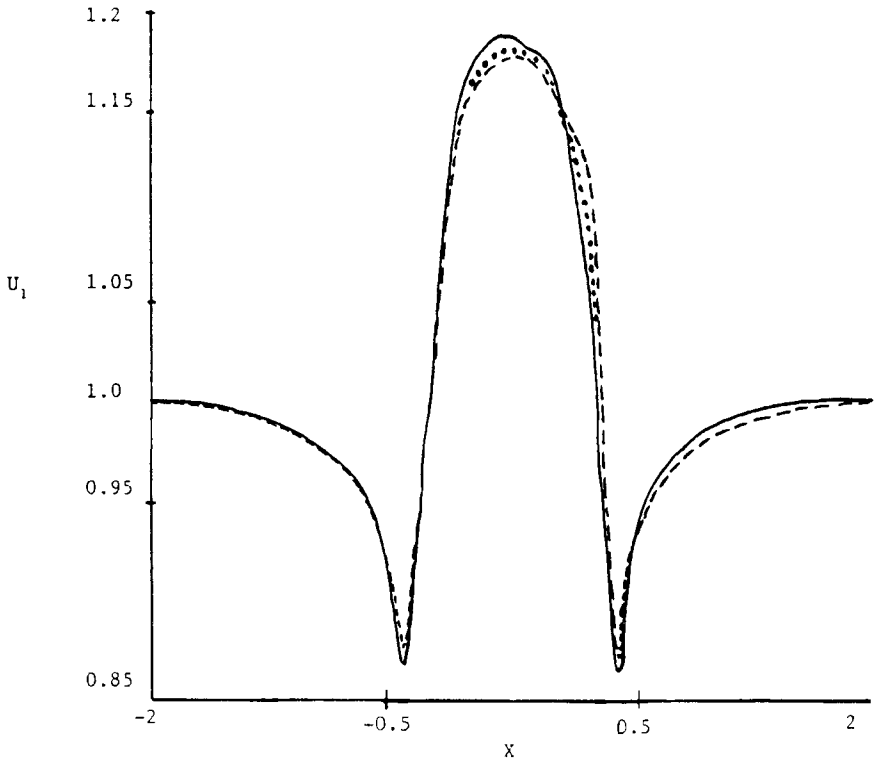

Figure 3. Fluid phase horizontal velocity component along the interface ($K_1=20$): – – – –, $\eta=0{\cdot}1$; · · · ·, $\eta=0{\cdot}01$; ———, $\eta=0{\cdot}001$

decrease in velocity with increasing K_1 is attributed to the fact that when the mass of each dust particle is considered constant, then increasing K_1 results in increasing the drag coefficient of resistance, which results in slowing down the dust particle motion as depicted in Figure 4.

For a given permeability $\eta=0{\cdot}01$ and $K_1=20$, Figure 5 illustrates the fluid phase normal component of velocity over the hump. This profile is representative of this fluid phase component for different K_1 and different permeabilities. The figure also gives the comparison at $K_1=20$ between the fluid phase and dust phase normal velocity components.

Figure 6 illustrates the fluid phase X-component of velocity along the vertical line passing through a point near the maximum of $f(X)$. The figure indicates that as the permeability is decreased for a given K_1, this velocity component decreases in regions away from the lower boundary. This behaviour is of course expected, as discussed above with regard to Figure 3. As we approach the upper regions of the flow domain, fluctuations of this component of velocity occur. For larger permeability this oscillation starts to dampen out. Although it is expected that at points far enough from the interface the profile should become more uniform, as indicated by the boundary conditions far upstream, this behaviour might be an indication that the extent of the flow domain is not large enough. The uppermost streamline might thus be viewed as a boundary line which, according to the flow condition of constant number density, perfectly reflects the dust particles back into the flow field. This in turn might result in the detected fluctuations and oscillations in velocity as depicted in Figure 6.

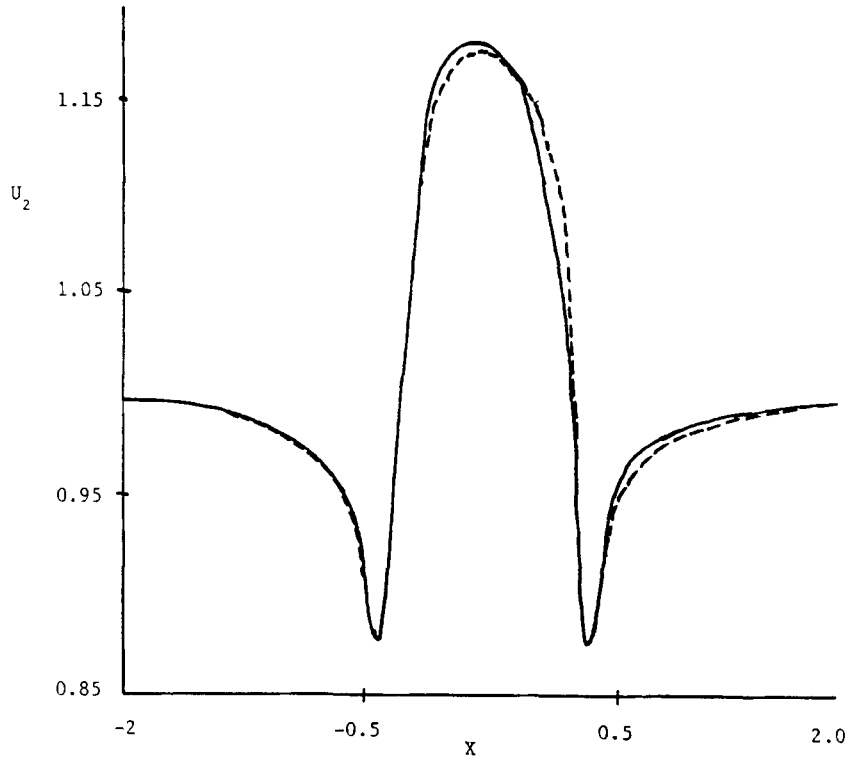

Figure 4. Dust phase horizontal velocity component along the interface ($\eta = 0{\cdot}1$): – – – –, $K_1 = 50$; ———, $K_1 = 20$

In the light of the effect of permeability on damping out the oscillations, it might also be concluded that the permeability associated with the dusty fluid flow model considered should be large. It has also been noticed that increasing K_1 results in damping out these oscillations for a given permeability.

8.3 Fluid phase vorticity

Figures 7 and 8 illustrate the fluid phase and dust phase vorticities along the static interface over the hump. In Figure 7 the vorticity is illustrated for $K_1 = 20$ and different permeabilities. From this figure one can conclude that the absolute value of vorticity decreases with decreasing permeability. In Figure 8 the fluid phase and dust phase vorticities along the static interface over the hump are compared. This figure indicates the increase in the dust phase vorticity over the fluid phase vorticity for a given value of permeability and a given K_1. As the value of K_1 is increased for a given permeability, the fluid phase and dust phase vorticities approach each other.

In both Figures 7 and 8 an appreciable drop in the vorticities is noticed as we move in the downstream direction, when $X > 0{\cdot}25$, and this drop becomes sharp as we approach the trailing edge of the hump. This of course may be ascribed to the fact that the far-downstream imposed condition is that of a uniform flow and thus it forces the vorticity to undergo drastic oscillations. Furthermore, this might also be indicative of the need for a finer grid or a clustered grid in regions close to the leading and trailing edges of the hump in order to obtain a more accurate solution.

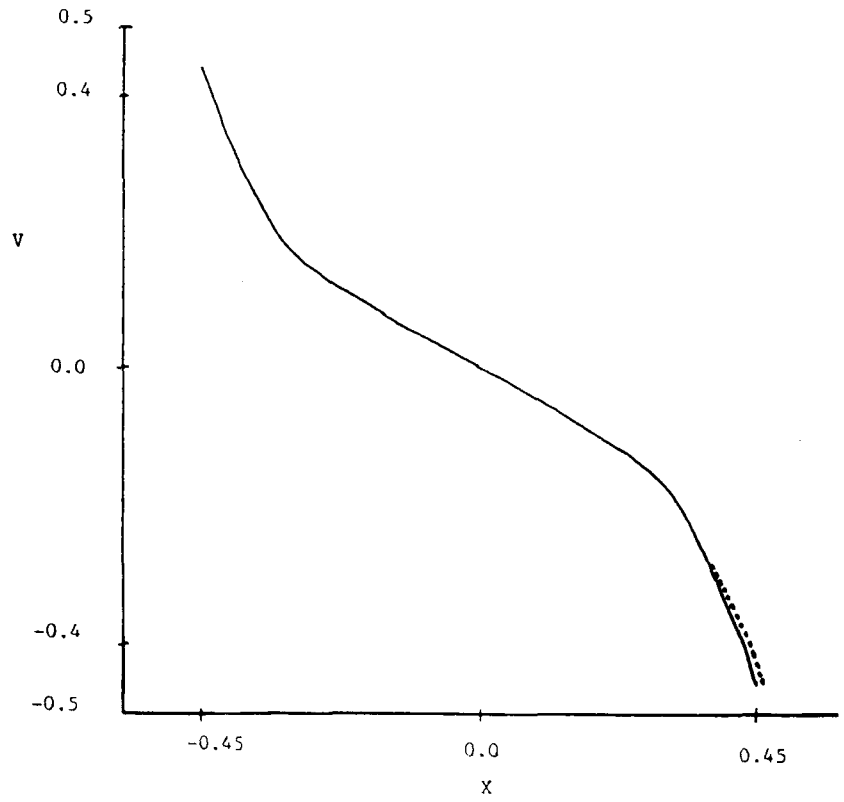

Figure 5. Fluid phase (———) and dust phase (· · · ·) vertical velocity components along the interface ($\eta = 0{\cdot}01$, $K_1 = 20$)

8.4. Grid refinement and domain extent

In order to illustrate the effects of the grid size and the domain extent on the convergence of the numerical procedure and on the computed results, a numerical experiment is carried out in which different mesh sizes are considered for a fixed domain extent and different domain extents for a fixed grid size. For the sake of simplicity the effect of the domain extent in the Y-direction is isolated in this experiment by considering the flow domain described by

$$-\infty < X < \infty, \qquad f_1(X) \leqslant Y \leqslant f_2(X),$$

where

$$f_1(X) = \begin{cases} 0{\cdot}2(0{\cdot}25 - X^2)^{1/2}, & -0{\cdot}5 \leqslant X \leqslant 0{\cdot}5, \\ 0, & X < -0{\cdot}5 \text{ or } X > 0{\cdot}5, \end{cases}$$

and

$$f_2(X) = \begin{cases} 1 - 0{\cdot}2(0{\cdot}25 - X^2)^{1/2}, & -0{\cdot}5 \leqslant X \leqslant 0{\cdot}5, \\ 1, & X < -0{\cdot}5 \text{ or } X > 0{\cdot}5. \end{cases}$$

This corresponds to the computational domain described by

$$-\infty < X < \infty, \qquad 0 \leqslant \Psi_1 = \Psi_2 \leqslant 1.$$

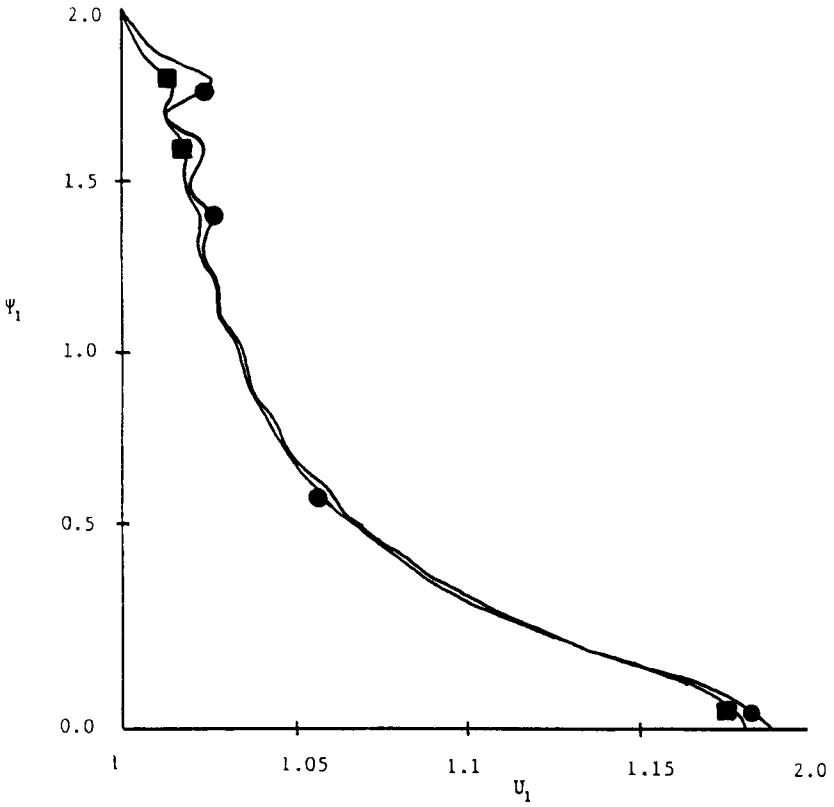

Figure 6. Fluid phase horizontal velocity component at $X = X_m$, corresponding to a point near the maximum of $f(X)$ ($K_1 = 20$): -■-■-, $\eta = 0{\cdot}01$; -●-●-, $\eta = 0{\cdot}001$

The boundary conditions associated with this problem are uniform flow at infinity for both phases and flow tangency along the boundaries.

Three different computational domain extents in the X-direction are considered: $X \in [-2, 2]$, $X \in [-3, 3]$ and $X \in [-4, 4]$. The results of the numerical experiment are summarized in Tables III–VII.

Table III illustrates the effect of the computational domain extent for different grid sizes and different permeabilities on the number of iterations required for convergence, with the convergence criterion being the same as that discussed in Section 7. The table shows that increasing the number of grid points for a given domain extent results in an increase in the number of iterations. This behaviour might be ascribed to the fact that it requires more 'effort' to dampen out the large oscillations in the solution in the case of a finer grid.

For a given grid size Table III also shows that increasing the domain extent results in a decrease in the number of iterations necessary for convergence. This may be seen in the table as one goes from $X \in [-2, 2]$ to $X \in [-3, 3]$ with the 64×22 grid and from $X \in [-3, 3]$ to $X \in [-4, 4]$ with the 84×22 grid.

Table IV illustrates the effect of permeability on the number of iterations for different grid sizes and different computational domain extents. In all cases it is seen that decreasing the permeability results in decreasing the number of iterations. This may be ascribed to the fact that the diagonal

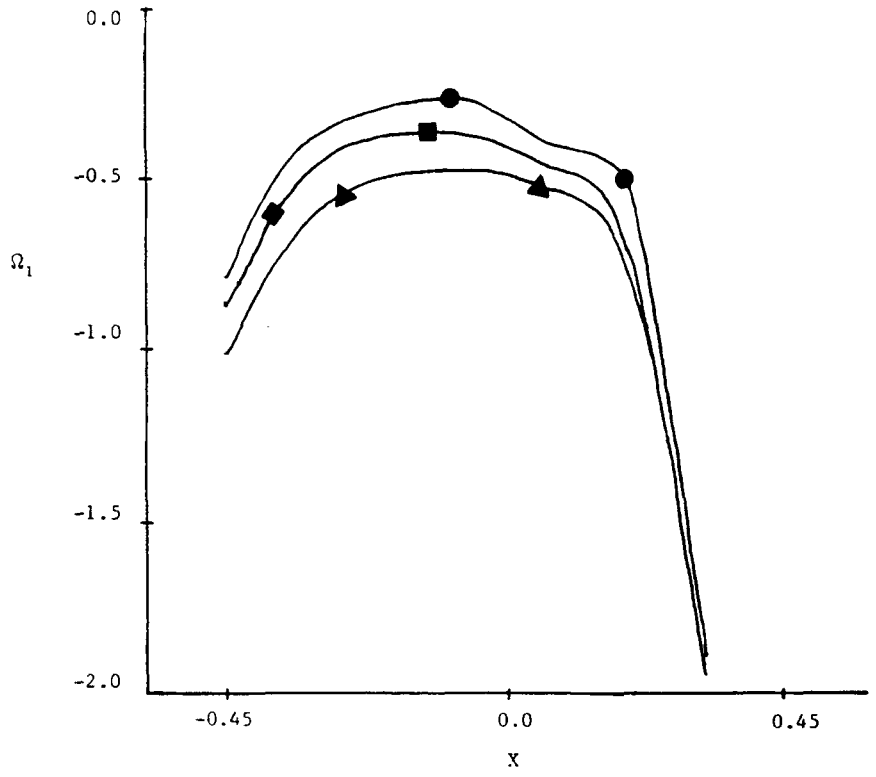

Figure 7. Fluid phase vorticity along the interface ($K_1 = 20$): -▲-▲-, $\eta = 0{\cdot}1$; -■-■-, $\eta = 0{\cdot}01$; -●-●-, $\eta = 0{\cdot}001$

dominance of the matrix resulting from the fluid phase vorticity equation is enhanced with a reduction in permeability, thus rendering faster convergence.

For a fixed domain extent Table V illustrates the effect of the grid size in the Ψ-direction on the number of iterations. It demonstrates the increase in the number of iterations with increasing number of grid points in the Ψ-direction, a conclusion that is consistent with the results in Table III.

The effects of the grid size and the extent of the computational domain on the computed results are illustrated in Tables VI and VII. These effects are studied on the fluid phase and dust phase tangential velocity components U_1 and U_2 respectively at the centre of the flow domain, $(X, Y) = (0, 0{\cdot}5)$. The values are obtained by averaging the values of U_1 and U_2 at the four grid points neighbouring the centre of the channel.

In all the cases considered the qualitative behaviour of the velocity components is the same, i.e. the dust phase velocity component is slightly greater than the fluid phase component. This of course sheds some light on the accuracy of the numerical scheme and the method employed. The quantitative behaviour, on the other hand, indicates slight discrepancies in the results with increasing domain extent and/or grid refinement. The error committed (maximum of the absolute and the relative), however, remains less than 3%, thus indicating that the coarse grid solution might serve as an acceptable first approximation to the solution.

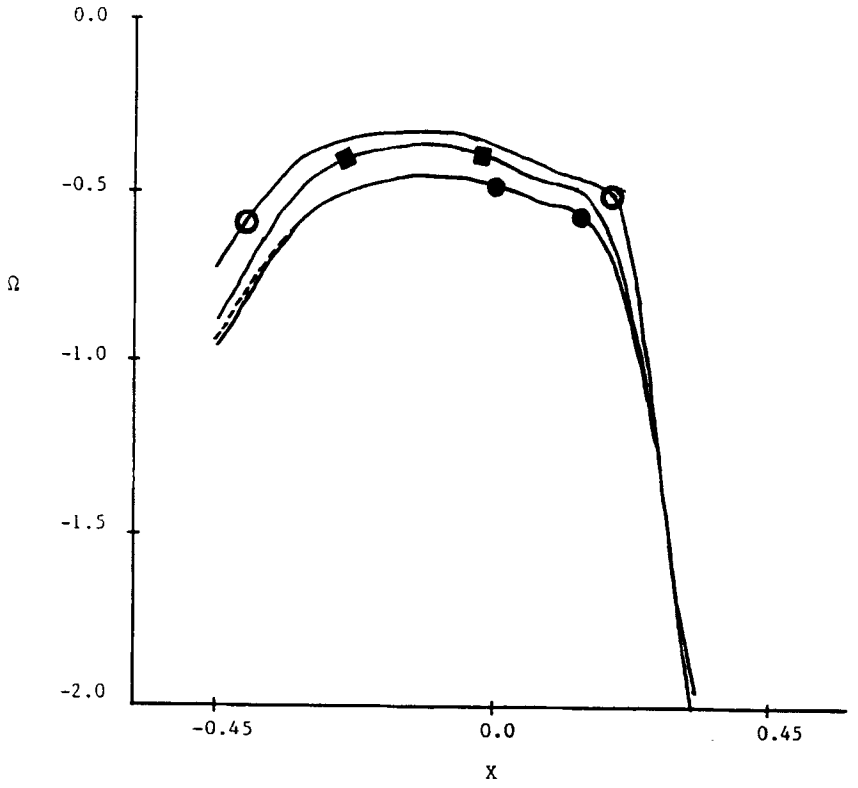

Figure 8. Fluid phase and dust phase vorticities along the interface ($\eta = 0{\cdot}01$): -●-●-, $K_1 = 50, \Omega_1$; - - - -, $K_1 = 50, \Omega_2$; -■-■-, $K_1 = 20, \Omega_1$; -○-○-, $K_1 = 20, \Omega_2$

Table III. Effect of the horizontal extent of the domain on the number of iterations ($K_1 = 20$)

$X \in$	Grid size	η	Iterations
[−4, 4]	100 × 22	0·1	219
		0·05	197
	84 × 22	0·1	157
		0·05	133
[−3, 3]	84 × 22	0·1	400
		0·05	381
	64 × 22	0·1	160
		0·05	138
[−2, 2]	32 × 22	0·1	127
	32 × 22	0·05	108
	52 × 22	0·05	194
	64 × 22	0·05	705

Table IV. Effect of permeability η on the number of iterations ($K_1 = 20$)

$X \in$	$[-2, 2]$	$[-3, 3]$	$[-3, 3]$	$[-4, 4]$	$[-4, 4]$
Grid	32×22	64×22	84×22	84×22	100×22
$\eta = 0{\cdot}05$	108	138	381	133	197
$\eta = 0{\cdot}1$	127	160	400	157	219

Table V. Effect of the grid size in the Ψ-direction on number of iterations ($X \in [-2, 2]$)

Grid size	η	K_1	Iterations
42×32	0·05	20	126
52×22			194
52×42			242
42×22	0·05	50	151
52×42			288
32×22	0·1	50	110
52×22			236
52×42			288

Table VI. Tangential velocity components at the centre of the channel for different grid sizes ($X \in [-2, 2]$, $K_1 = 20$)

Grid size	U_1	U_2
32×22	0·85447	0·85817
52×22	0·87057	0·87202
42×32	0·85822	0·85861
52×42	0·87413	0·87475

Table VII. Fluid phase and dust phase velocity components at the centre of the channel for different grid sizes, domain extents and permeabilities ($K_1 = 20$)

Grid size and domain	Permeability η	U_1	U_2
100×22	0·05	0·86402	0·86542
$[-4, 4]$	0·1	0·86454	0·86601
84×22	0·05	0·86574	0·86692
$[-4, 4]$	0·1	0·86618	0·86742
84×22	0·05	0·85879	0·85885
$[-3, 3]$	0·1	0·85917	0·85945
64×22	0·05	0·86861	0·86981
$[-3, 3]$	0·1	0·86904	0·87029

9. CONCLUSIONS

In this work the von Mises transformation has been extended in terms of double co-ordinates in an attempt to provide a method that is applicable to the study of general two-phase flow over curved boundaries. The transformation has also been implemented in the study of dusty fluid flow through a porous medium bounded below by a stationary fluid. The nature of the problem considered does not allow for definitive conclusions about the employed model but illustrates how the double von Mises transformation may be utilized in the study of dusty fluid flow over curved boundaries. However, application of the method to more realistic flow problems will not only demonstrate the usefulness of the proposed method but will also give a greater insight on the possibility of implementing the method and demonstrating its advantages, some of which are summarized as follows.

1. In the study of dusty gas flows over curved boundaries which are streamlines, the extended von Mises transformation offers a simple and plausible way to handle the curved boundaries provided that the spatial Jacobians of the transformations remain finite and do not vanish. The method has proven to be easy to implement numerically and is easy to code.
2. In cases where the number density N is not taken to be constant, it is possible to determine the regions of dust accumulation by the knowledge of the shape of the dust phase streamlines which are directly obtained by plotting the values of Y_2 for a given Ψ_2.
3. The method is not restricted to dusty fluid flow through porous media. It is easily implemented for the usual dusty gas flow equations in free space.
4. The method is not restricted to the study of dusty gas flows over curved boundaries. It can also be used in the case of straight boundaries, when N is variable, and thus regions of dust accumulation may be determined as in point 2 above.

APPENDIX: NOMENCLATURE

Ψ	dimensionless streamfunction
Ψ_1	dimensionless first-phase streamfunction
Ψ_2	dimensionless second-phase streamfunction
σ	typical streamline (constant streamfunction)
Ω	dimensionless vorticity
Ω_1	dimensionless first-phase voritcity
Ω_2	dimensionless second-phase vorticity
Φ, Φ_1, Φ_2	curvilinear co-ordinates
τ, τ_1, τ_2	time variables in the von Mises and extended von Mises transformations
$X, Y, X_1,$ Y_1, X_2, Y_2	dimensionless Cartesian co-ordinates
T, T_1, T_2	dimensionless time variables
J_1, J_{1S}, J_{2S}	spatial Jacobians of transformation
J_2, J_{1T}, J_{2T}	temporal Jacobians of transformation
n, N	dust particle number densities
m, M	masses of single dust particles
S	Stokes coefficient of resistance ($S = 6\pi r\mu$ when the dust particles are spheres of radius r)
K	drag coefficient of resistance in the porous medium
K_1	$K/(mL/U_0)$
ρ	fluid density

μ	fluid viscosity
η^*	dimensional permeability
η	dimensionless permeability
f, f_1, f_2	functions of X
p	fluid phase partial pressure
p^*	dust phase partial pressure
L	length, reference length
U_0	characteristic velocity
Re	Reynolds number
$\mathbf{v}$	dust phase velocity vector
$\mathbf{u}$	fluid phase velocity vector
$\mathbf{V}$	dust phase dimensionless velocity vector
$\mathbf{U}$	fluid phase dimensionless velocity vector
U_1, V_1	fluid phase velocity components
U_2, V_2	dust phase velocity components
U, V	dimensionless velocity components

REFERENCS

1. C. T. Crowe, 'Review—numerical models for dilute gas–particle flows', *J. Fluids Eng.*, **104,** 297–303 (1982).
2. S. L. Soo, *Fluid Dynamics of Multiphase Systems*, Blaisdell, Waltham, MA, 1967, p. 467.
3. M. H. Hamdan and R. M. Barron, 'A dusty gas flow model in porous media', *J. Comput. Appl. Math.*, **30,** 21–37 (1990).
4. R. von Mises, 'Bemerkungen zur Hydrodynamik', Z. Angew. Math. Mech., **7,** 425–429 (1927).
5. D. Meksyn, *New Methods in Laminar Boundary-Layer Theory*, Pergamon, New York, 1961, Chap. 2.
6. T. B. Benjamin, 'The solitary wave on a stream with an arbitrary distribution of vorticity', *J. Fluid Mech.*, **12,** pt. 1, 97–115 (1961).
7. R. M. Barron, 'Computation of incompressible potential flow using von Mises coordinates', *Math. Comput. Simul.*, **31,** 177–188 (1989).
8. M. H. Martin, 'The flow of a viscous fluid. I', *Arch. Rat. Mech. Anal.*, **41,** 266–286 (1971).
9. M. H. Hamdan, 'Numerical simulation of flow through porous media', *Ph.D. Dissertation*, Applied Mathematics, FDRI, University of Windsor, Ontario, 1989, Chap. 6.
10. P. G. Saffman, 'On the stability of laminar flow of a dusty gas', *J. Fluid Mech.*, **13,** pt. 1, 119–128 (1962).
11. R. M. Barron and M. H. Hamdan, 'The structure of separated dusty gas flow at low and moderate *Re*', *Int. J. Eng. Sci.*, **27,** 261–276 (1989).
12. B. C. Chandrasekhara, Rajani Kantha and N. Rudraiah, 'Effect of slip on porous-walled squeeze films in the presence of a transverse magnetic field', *Appl. Sci. Res.*, **34,** 393–411 (1978).